iScience

CellPress
OPEN ACCESS

Article

A purinergic mechanism underlying metformin regulation of hyperglycemia

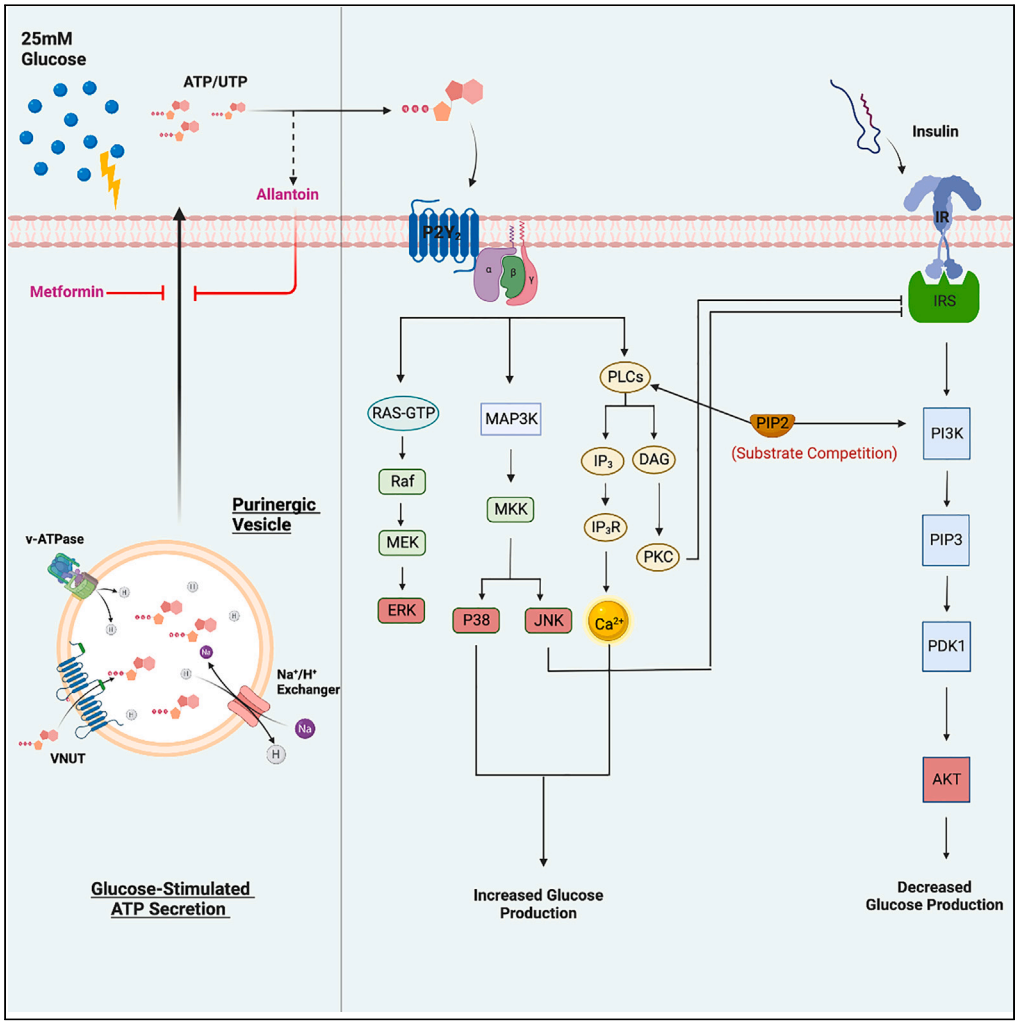

Jared Senfeld, Qianman Peng, Yi Shi, Shenqi Qian, Jianzhong Shen

jzs0019@auburn.edu

Highlights

High glucose stimulates hepatocyte secretion of ATP via the endolysosomal system

ATP-activated $P2Y_2R$ inhibits insulin-AKT signaling leading to glucose dyshomeostasis

Metformin and other antidiabetic biguanides suppress glucose-stimulated ATP secretion

Metformin's antihyperglycemic effect is abrogated in $P2Y_2R$-deficient mice

Senfeld et al., iScience 26, 106898
June 16, 2023
https://doi.org/10.1016/j.isci.2023.106898

iScience

CellPress
OPEN ACCESS

Article

A purinergic mechanism underlying metformin regulation of hyperglycemia

Jared Senfeld,[1,2] Qianman Peng,[1,2] Yi Shi,[1] Shenqi Qian,[1] and Jianzhong Shen[1,3,*]

SUMMARY

Metformin, created in 1922, has been the first-line therapy for treating type 2 diabetes mellitus for almost 70 years; however, its mechanism of action remains controversial, partly because most prior studies used supratherapeutic concentrations exceeding 1 mM despite therapeutical blood concentrations of metformin being less than 40 μM. Here we report metformin, at 10–30 μM, blocks high glucose-stimulated ATP secretion from hepatocytes mediating its antihyperglycemic action. Following glucose administration, mice demonstrate increased circulating ATP, which is prevented by metformin. Extracellular ATP through $P2Y_2$ receptors ($P2Y_2R$) suppresses PIP_3 production, compromising insulin-induced AKT activation while promoting hepatic glucose production. Furthermore, metformin-dependent improvements in glucose tolerance are abolished in $P2Y_2R$-null mice. Thus, removing the target of extracellular ATP, $P2Y_2R$, mimics the effects of metformin, revealing a new purinergic antidiabetic mechanism for metformin. Besides unraveling long-standing questions in purinergic control of glucose homeostasis, our findings provide new insights into the pleiotropic actions of metformin.

INTRODUCTION

The global prevalence of obesity and type 2 diabetes mellitus (T2DM) surmounts to epidemic proportions and is expected to afflict over 700 million people by 2045.[1] Generated in 1922[2] and used for almost 70 years, metformin is a first-line pharmacotherapy taken by over 150 million patients worldwide to improve glycemic control. Metformin effectively suppresses hepatic glucose production and enhances insulin sensitivity[3]; however, its mechanism of action (MOA) remains enigmatic. It has been reported that metformin inhibits mitochondrial complex I, disrupting respiration at doses exceeding therapeutically achievable concentrations.[4,5] Another documented MOA was that metformin stimulates AMPK, which has recently been brought into question because metformin's antidiabetic capabilities were unaffected in liver-specific AMPK knockout (KO) mice.[6] We also found that metformin up to 30 μM neither changed intracellular total ATP levels nor activated AMPK in human hepatocytes (Figure S1). Further, forced expression of gluconeogenic genes, including *glucose-6-phosphatase*, failed to affect the suppression of hepatic gluconeogenesis by metformin.[6] Therefore, we may reasonably conclude that metformin operates, in part, in an AMPK- and transcriptional-independent manner. Unlike other antidiabetic medicines, metformin seldom affects normal fasting blood glucose levels,[7] leading us to consider that metformin's MOA may rely on physiological events initiated during increased blood glucose concentrations. Thus, we examined the hyperglycemia-induced MOA of metformin.

RESULTS AND DISCUSSION

Antidiabetic biguanides suppression of glucose-stimulated ATP secretion (GSAS)

Extracellular high glucose is a chemical stressor, inducing ATP release from various metabolic tissues, including the liver.[8,9] Thus, we proposed that GSAS represents an autocrine and paracrine mechanism that insulin-sensitive tissues employ to control glucose homeostasis through the purinergic signaling axis. Figure 1A shows that challenging HepG2 human hepatocytes with 25 mM glucose, but not by 25 mM mannitol, induced time-dependent ATP secretion, indicative of a specific GSAS in hepatocytes. Interestingly, co-treatment of the cells with 30 μM metformin abolished GSAS in all tested time points (Figure 1A), which was not due to a change in extracellular glucose level (Figure S2). Further studies indicated that the minimum effective concentration of metformin to block GSAS is around 10 μM (Figure 1B),

[1]Department of Drug Discovery and Development, Harrison College of Pharmacy, Auburn University, Auburn, AL 36849, USA

[2]These authors contributed equally

[3]Lead contact

*Correspondence: jzs0019@auburn.edu

https://doi.org/10.1016/j.isci.2023.106898

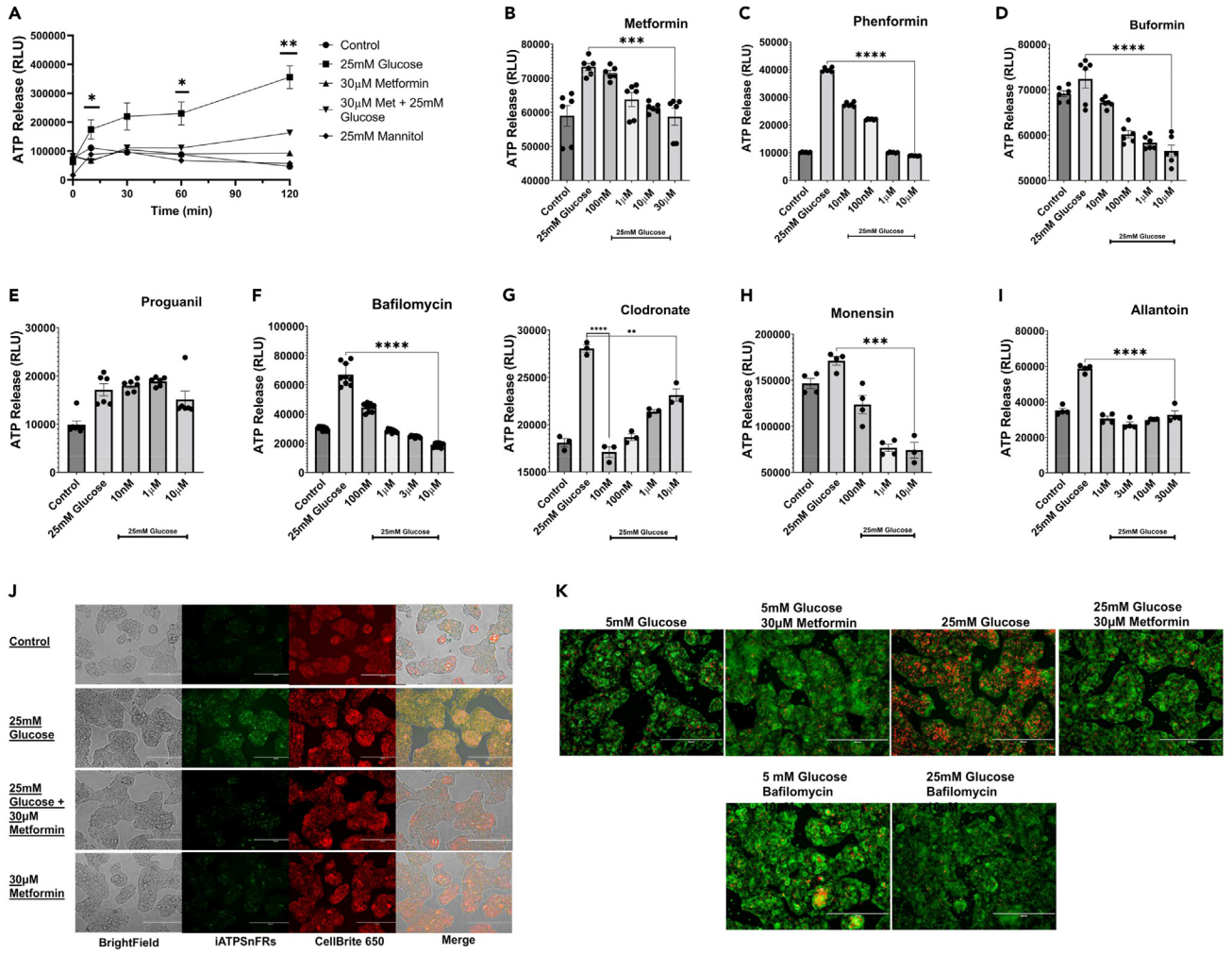

Figure 1. Metformin, alongside other biguanides and endolysosomal alkalizing agents, prevents glucose-stimulated ATP secretion (GSAS)

(A) Time course observation of ATP secretion originating from HepG2 hepatocytes treated with 5.5 mM (control), 25 mM glucose, or 25 mM mannitol with or without co-treatment with 30 μM metformin. Data are means ± SEM of four independent experiments. *p < 0.05, **p < 0.01, evaluated by unpaired two-tailed Student's *t* test.

(B–I) Dose-dependent effects on GSAS by antidiabetic biguanides metformin, phenformin, buformin, antimalaria biguanide proguanil, endolysosomal targeting agents bafilomycin, clodronate, monensin, and ATP metabolite allantoin. Data are means ± SEM of three independent experiments. ***p < 0.005, ****p < 0.001,evaluated by unpaired two-tailed Student's *t* test.

(J) Detection of extracellular ATP signal (green) by HepG2 cells transfected with iATPSnFR, a plasma membrane-bound ATP sensor, was observed following the indicated treatments and co-localized with a cell membrane red dye Cellbrite650 (yellow).

(K) Effect of metformin and high glucose treatment on endolysosomal pH change monitored by LysoView633 (red), a pH-sensitive endolysosomal probe. CellBrite488 (green) was used for plasma membrane staining, and bafilomycin as a positive control. Shown are representative of three independent experiments. Scale bar: 200 μm. See also Figures S1–S8, S16, and S18.

consistent with the known clinical blood concentration range of 10–40 μM for metformin.[10] Importantly, this GSAS-blocking effect was fully mimicked by phenformin and buformin at a much higher potency (Figures 1C and 1D) and fully replicated in primary human hepatocytes (Figure S3), consistent with their clinical dose profiles. In contrast, proguanil, an analog of metformin with no antidiabetic effect, had no inhibition on GSAS (Figure 1E). To complement our luciferase ATP assays not interfered with by metformin at 30 μM (Figure S4), we generated a HepG2 cell line in which the cell membrane stably expressed a fluorescent sensor detecting extracellular ATP (iATPSnFR). Figure 1J shows that, compared with control 5.5 mM glucose, treatment of HepG2-iATPSnFR cells with 25 mM glucose for 60 min exhibited more green fluorescent signals co-localized with the cell membrane red fluorescence. Co-treatment of the cells with 30 μM metformin abolished the green fluorescence, indicating that metformin suppresses GSAS

(Figures 1J and S5), which was further confirmed by another different fluorometric ATP quantification assay (Figure S6).

Vesicular origin of GSAS targeted by metformin

We then explored the origin of ATP released in response to hyperglycemia. Curiously, metformin's primary site of action, the liver, expresses significantly more vesicular nucleotide transporters (VNUTs) mRNA than any other tissue in the human body,[11] and we confirmed its cytoplasmic expression in HepG2 cells (Figure S7). VNUT-KO mice demonstrated improved glucose tolerance and insulin sensitivity.[12,13] Further, VNUT activity is coupled with the action of V-type-ATPase that has recently been implicated in the MOA of metformin.[14] Therefore, we first considered a vesicular origin of GSAS. To evaluate the contribution of the endolysosomal system, we pharmacologically depleted endolysosome ATP content by disruption of the proton gradient or by inhibition of the ATP transporter. Pretreatment of the cells with clodronate or bafilomycin, VNUT, and V-type-ATPase inhibitors produced a dose-dependent reduction in GSAS (Figures 1F and 1G). Consistent with this, pretreatment of the cells with monesin, a chemical mimetic of Na^+/H^+ exchanger known to alkalize the luminal pH of endolysosomes, reduced GSAS (Figure 1H). In addition, we verified that high glucose treatment acidified endolysosomes, as evidenced by increased LysoView pH-dependent probe staining, which was suppressed by 30 μM metformin (Figure 1K). Thus, our results support the notion that metformin may interfere with the proton gradient of the endolysosome, leading to the depletion of vesicular ATP content, which was further supported by our observation that metformin prevented MANT-ATP accumulation (Figure S8). We then hypothesized that a metabolite of the purine degradation pathway might serve as an endogenous feedback mechanism to control GSAS. Allantoin, a metabolite of uric acid negatively correlated with T2DM,[15,16] displayed potent inhibition of GSAS at physiological concentrations (Figure 1I). However, humans harbor a loss-of-function mutation in the gene encoding uric oxidase; consequently, humans cannot convert uric acid to allantoin enzymatically, potentially predisposing modern humans to diabetes.

$P2Y_2R$ inhibition of insulin-AKT signaling

Next, we aimed to define how extracellular ATP affects hepatocyte metabolic signaling, focusing on the nucleotide P2Y receptors (P2Y2R) since the adipocyte $P2Y_6$ and $P2Y_{14}$ receptors are implicated in metabolic disease.[17,18] RT-PCR analysis indicated that $P2Y_2$ and $P2Y_{11}$ are the predominant ATP-sensitive P2Y receptors expressed in HepG2 cells (Figure 2A). Ca^{2+} mobilization assays showed that both ATP and UTP induced a dose-dependent increase of intracellular Ca^{2+}, which was abolished by ARC-118925XX, a $P2Y_2R$-selective antagonist (Figures 2B–2D), and no functional $P2Y_6R$ and $P2Y_{11}R$ were detected (Figure S9). Small interfering RNA (siRNA) silencing of the $P2Y_2R$ also abolished ATP- or UTP-induced Ca^{2+} signaling (Figure 2E), supporting $P2Y_2R$ as the primary ATP- and UTP-sensitive P2Y receptor in hepatocytes. We then explored $P2Y_2R$-mediated other signaling pathways. Figures 2F and S10 show that stimulation of the $P2Y_2R$ activated the JNK and p38 pathways with slight activation of the ERK1/2 and no activation of the AKT pathways. Activation of JNK and p38 pathways indicates an inflammatory response, a condition often preceding metabolic dyshomeostasis and insulin resistance.[19–21]

Further, the apparent decrease of basal AKT phosphorylation by ATP and UTP made us hypothesize that the $P2Y_2R$ may have an inhibitory effect on the AKT pathway. This was supported by our finding that ATP and UTP dose-dependently suppressed insulin-induced AKT phosphorylations at the T308 and S473 sites (Figures 2G and 2H) without compromising the ERK1/2 pathway (Figure S11). The expression and function of $P2Y_2R$ in control of insulin-AKT signaling were also confirmed in primary human hepatocytes (Figures S12 and S13). To further explore the underlying mechanism(s) responsible for $P2Y_2R$-mediated AKT inhibition, we hypothesized that depletion of PIP_2, a substrate shared by PI3K and PLC, may be involved. Figure 2I shows that activation of the $P2Y_2R$ decreased insulin-induced AKT phosphorylation, which was entirely prevented by U73122, a specific PLC inhibitor. In addition, stimulation of the $P2Y_2R$ suppressed insulin-induced PIP_3 generation (Figure S14), and supplementation of PIP_2 at least partially rescued $P2Y_2R$-mediated AKT inhibition (Figure S15). These results indicate that $P2Y_2R$ selectively impairs insulin-induced AKT signaling, consistent with numerous reports that insulin resistance and T2DM are linked to a disruption of a branch of insulin receptor signaling. Further, identifying $P2Y_2R$ as the anti-insulin signaling mediator advances early discoveries demonstrating potent inhibition of insulin signaling and hepatocyte glucose production by extracellular nucleotides.[22–29] All these shreds of evidence support our hypothesis that metformin improves hepatic insulin sensitivity by suppressing ATP release and signaling, consistent with a previous

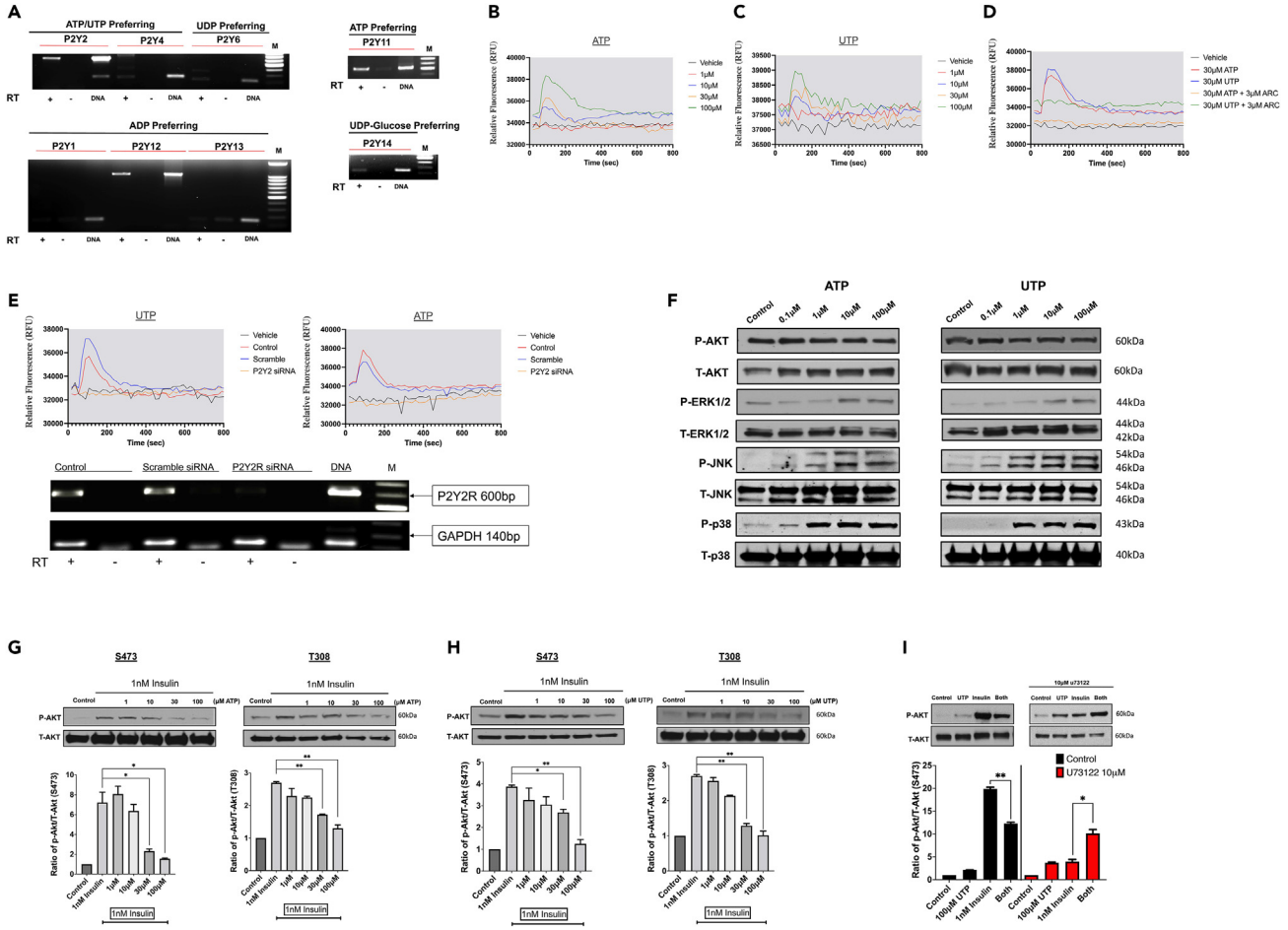

Figure 2. Identification of AKT-inhibitory purinergic P2Y$_2$R in hepatocytes

(A) RT-PCR analysis of mRNA expression profile of the eight known P2Y receptor subtypes in HepG2 cells.

(B and C) HepG2 cells were stimulated with P2Y$_2$R agonists ATP and UTP at the indicated concentrations, and [Ca^{2+}]i mobilization was monitored fluorometrically.

(D) Effect of P2Y$_2$R-selective antagonist ARC-118925XX (3 μM, 45 min) on nucleotide-induced [Ca^{2+}]i mobilization.

(E) Hepatocytes were pretreated for 48 h with P2Y$_2$R siRNA (50 nM) or scrambled siRNA (50 nM), and nucleotide-induced [Ca^{2+}]i mobilization was assessed. P2Y$_2$R knockdown was confirmed through RT-PCR.

(F) Western blotting was employed to determine P2Y$_2$R signaling to the MAPK and AKT pathways following a 10 min stimulation by ATP or UTP at the indicated doses.

(G and H) Effect of P2Y$_2$R stimulation on insulin-induced AKT phosphorylations at the sites of T308 and S473. The data shown are representative of three independent experiments. *$p < 0.05$, **$p < 0.01$, evaluated by unpaired two-tailed Student's *t* test.

(I) Effect of PLC-selective inhibitor U73122 (10 μM, 45 min) on P2Y$_2$R-mediated suppression of insulin-AKT signaling. The data shown are representative of three independent experiments. *$p < 0.05$, **$p < 0.01$, evaluated by unpaired two-tailed Student's *t* test. See also Figures S9–S15 and S17.

report utilizing insulin receptor-null mice concluding that "for metformin to have any effect, an operating insulin-signaling system in the liver is mandatory."[30]

P2Y$_2$R promotes hepatocyte glucose production (HGP)

We then assessed whether P2Y$_2$R affects HGP. Unlike skeletal muscle and adipose tissues, the primary hepatic glucose transporter, GLUT2, activity is not dependent on insulin signaling, enabling the liver to take in and release glucose bidirectionally during the fed and fasted state.[31] It was reported that intravenous administration of adenine nucleotides stimulates HGP.[23,25,26,32] However, a nucleotide receptor controlling HGP remained elusive; therefore, we first stimulated hepatocyte P2Y$_2$R with ATP and UTP, finding a dose-dependent reduction in glucose uptake (Figures 3A and 3B), suggesting a possible glucose release through GLUT2 in response to P2Y$_2$R activation. We then monitored gluconeogenesis

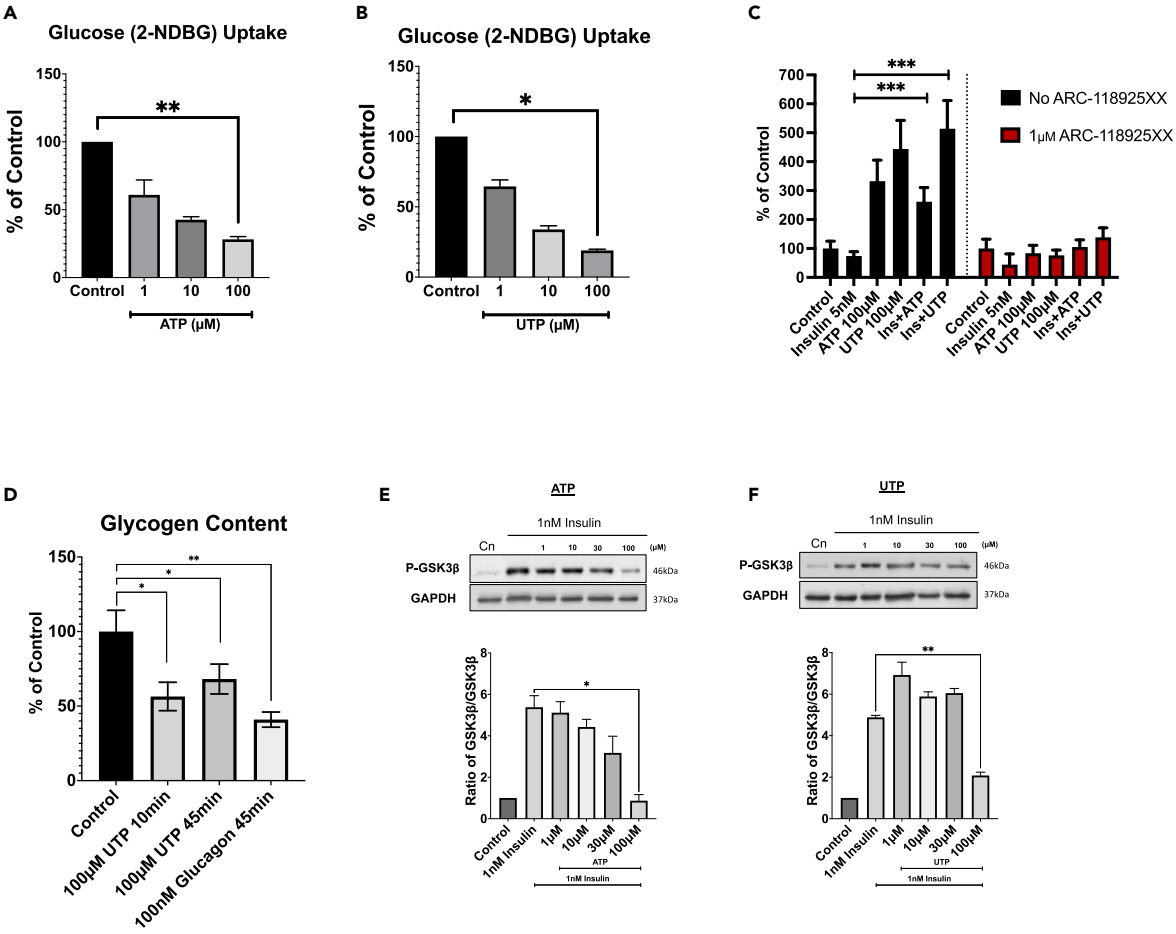
A
Glucose (2-NDBG) Uptake
% of Control
ATP (μM)
Control
1
10
100
B
Glucose (2-NDBG) Uptake
% of Control
UTP (μM)
C
No ARC-118925XX
1μM ARC-118925XX
% of Control
Control
Insulin 5nM
ATP 100μM
UTP 100μM
Ins+ATP
Ins+UTP
D
Glycogen Content
% of Control
Control
100μM UTP 10min
100μM UTP 45min
100nM Glucagon 45min
E
ATP
1nM Insulin
P-GSK3β
GAPDH
46kDa
37kDa
Ratio of GSK3β/GSK3β
F
UTP
1nM Insulin
P-GSK3β
GAPDH
Ratio of GSK3β/GSK3β

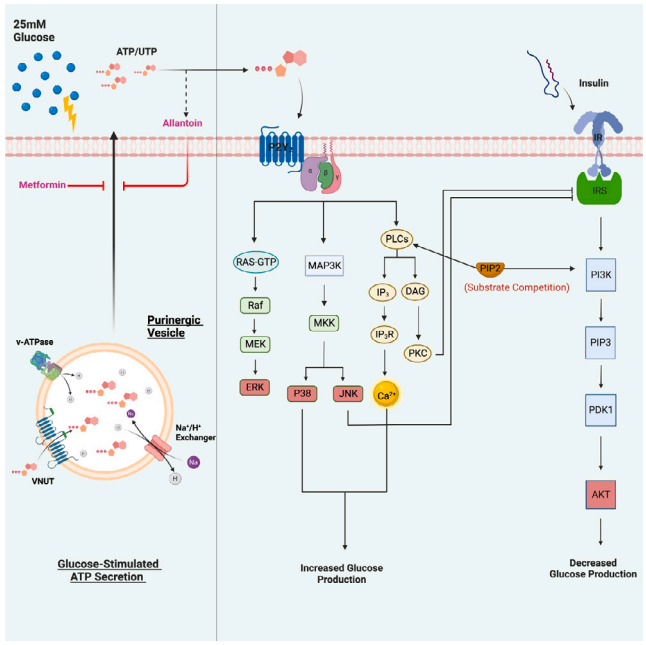
G
25mM Glucose
ATP/UTP
Allantoin
Metformin
Purinergic Vesicle
v-ATPase
VNUT
Na+/H+ Exchanger
Glucose-Stimulated ATP Secretion
Insulin
IR
IRS
PLCs
PIP2
(Substrate Competition)
PI3K
PIP3
PDK1
AKT
RAS-GTP
Raf
MEK
ERK
MAP3K
MKK
P38
JNK
IP3
DAG
IP3R
PKC
Ca2+
Increased Glucose Production
Decreased Glucose Production

Figure 3. $P2Y_2R$ control of hepatocyte glucose production

(A and B) HepG2 cells were stimulated with ATP or UTP at the indicated concentrations for 20 min; then 2-NDBG (150 μg/mL) was added for 10 min before quantifying intracellular 2-NDBG. *$p < 0.05$, **$p < 0.01$, n = 5. Unpaired two-tailed Student's *t* test.

(C) Hepatocyte gluconeogenesis was measured by an Amplex red coupled reaction following a 3.5-h simulation with ATP or UTP (100 μM) or insulin (1 nM) using 10 mM sodium lactate as gluconeogenic substrate. All cells were pretreated for 45 min with ARL-67156 (100 μM) to prevent nucleotide degradation and with or without ARC-118925XX (1 μM) as indicated. ***$p < 0.005$, n = 5. Unpaired two-tailed Student's *t* test.

(D) Hepatocyte glycogen content was measured fluorometrically following stimulation with UTP (100 μM) or glucagon (100 nM) for the indicated duration of time. *$p < 0.05$, **$p < 0.01$, n = 5. Unpaired two-tailed Student's *t* test.

(E and F) Insulin-induced inhibition of GSK3β by phosphorylation (S9) was assessed by western blotting after 10 min co-stimulation with ATP or UTP and insulin at the indicated concentrations. *$p < 0.05$, **$p < 0.01$, n = 5. Unpaired two-tailed Student's *t* test.

(G) A diagram shows a new fine-tuning GSAS mechanism underlying $P2Y_2R$-controlled insulin signaling, glucose production, and its pharmacological intervention by metformin in hepatocytes.

to determine if decreased glucose uptake was correlated with increased glucose production. Figure 3C shows that stimulating the HepG2 cells by ATP or UTP significantly increased gluconeogenesis. Notably, insulin failed to suppress nucleotide-induced gluconeogenesis (Figure 3C). However, pretreatment with the selective $P2Y_2R$ antagonist, ARC-118925XX, effectively prevented nucleotide-induced gluconeogenesis (Figure 3C). Early studies found that perfusing murine livers with ATP or UTP increased glycogen phosphorylase activity and glycogenolysis.[22,27,29] In line with these findings, we found that stimulation of the $P2Y_2R$ for 10 min or 45 min significantly decreased glycogen content in HepG2 cells, an effect comparable to that induced by a maximal dose of glucagon (Figure 3D). In addition, $P2Y_2R$ activation inhibited insulin-induced phosphorylation of GSK3β (Figures 3E and 3F), providing another layer of mechanistic understanding of $P2Y_2R$ control of insulin signaling and glycogen synthesis in hepatocytes as summarized in Figure 3G.

$P2Y_2R$ is required for metformin-induced antihyperglycemic action

Finally, we determined whether metformin's antihyperglycemic action *in vivo* is related to $P2Y_2R$. Animal studies indicate that CD39 deletion results in a hepatic insulin-resistant phenotype in mice,[33] and hyperglycemia decreases gene expression and activity of ectonucleotidases,[34] suggesting that hyperglycemia may potentiate liver purinergic signaling. Indeed, circulating adenine nucleotides were elevated in T2DM patients,[35] and intraperitoneal injection of AMP increased mouse blood ATP and glucose levels.[26] In db/db mice, elevated plasma adenine nucleotides strongly correlated with increased plasma glucose levels.[32] Prompted by these observations and our own *in vitro* findings, we determined whether glucose loading affects the blood level of ATP. Figure 4A shows that intraperitoneal administration of glucose significantly increased blood ATP levels at 30 min and 60 min, which were diminished considerably by metformin pretreatment at 50 mg/kg (intravenous [i.v.]), a mode of administration and dose shown to reach mouse plasma metformin concentrations around 10–20 μM within the first hour.[36] We then performed glucose tolerance test (GTT) and insulin tolerance test (ITT) assays in mice fed with a standard chow diet. Figure 4B shows that $P2Y_2R$-null (KO) mice exhibited a better glucose tolerance compared with littermate-controlled wild-type (WT) mice, and this effect was mimicked by metformin treatment in WT but not in KO mice (Figures 4C and 4D). Since a recent report indicated that mice lacking $P2Y_2R$ are resistant to diet-induced obesity and display improved glucose and insulin tolerance,[26] we compared ITT profiles in mice fed with a high-fat diet versus a regular diet. Figure 4F shows that metformin treatment significantly improved insulin tolerance in WT mice fed a high-fat diet. In contrast, the same metformin treatment did not impact insulin sensitivity in WT mice fed a standard chow diet (Figure 4E) and in KO mice fed a high-fat diet (Figure 4G). Further, we confirmed that liver $P2Y_2R$ and VNUT were upregulated in mice fed a high-fat diet compared to normal healthy mice (Figure 4H). These data support our notion that metformin's action relies on the presence of hyperglycemia and $P2Y_2R$.

We have demonstrated that metformin, alongside other antidiabetic biguanides, prevents hepatic GSAS and displays no antihyperglycemic effect in $P2Y_2R$-null mice, indicating that metformin's MOA involves disruption of the purinergic signaling axis. Hormones, glucagon, and insulin have been exhaustively studied due to their paramount roles in systemic metabolic homeostasis; however, nucleotide release could represent a transient and local mechanism employed by insulin-sensitive tissues in response to nutrient overload operating synergistically and competitively toward glucagon and insulin, respectively. Normalizing pathological nucleotide release could clarify the beneficial phenotypes of metformin treatment spanning diabetes, obesity-induced inflammation, aging, and other metabolically rooted pathologies.

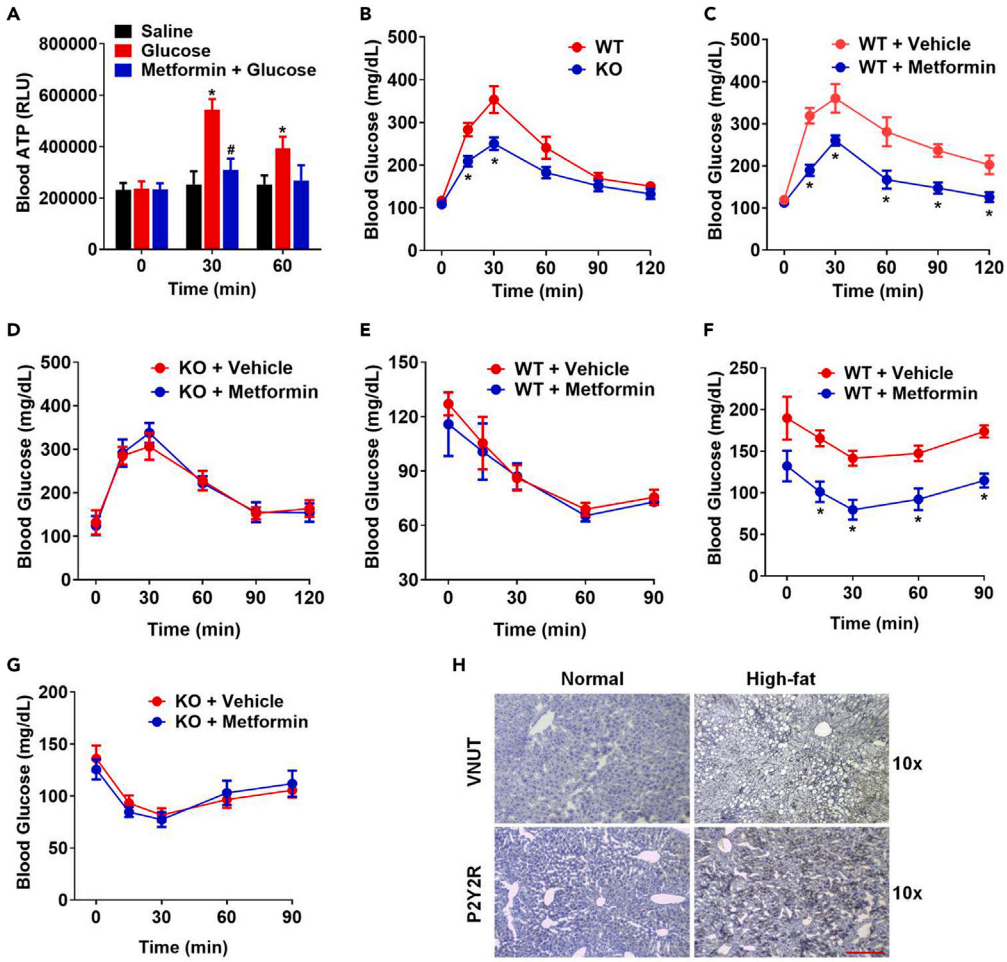

Figure 4. Hyperglycemia and P2Y$_2$R dictate metformin's antihyperglycemic action

(A) Effect of high glucose loading (1.5g glucose/kg, i.p.) on the relative levels of mouse blood ATP at the indicated times. WT mice were pretreated for 15 min with saline or metformin (50 mg/kg, i.v.) through tail vein injection before glucose loading. n = 6 mice in each group. *p < 0.05 compared with the saline group; #p < 0.05 compared with the glucose group. One-way analysis of variance, followed by unpaired two-tailed Student's *t* test.

(B–D) Glucose tolerance test (GTT, 1.5g glucose/kg, i.p.) comparing P2Y$_2$R-KO versus WT mice, metformin treatment (50 mg/kg, i.v.) versus saline in WT or P2Y$_2$R-KO mice on a standard chow diet. n = 6–10, *p < 0.05. Unpaired two-tailed Student's *t* test.

(E) Insulin tolerance test (ITT, 0.75 IU insulin/kg, i.p.) comparing vehicle- versus metformin-treated mice on a standard chow diet. n = 6–9.

(F and G) ITT was comparing saline versus metformin treatment on WT or P2Y$_2$R-KO mice fed with a high-fat diet for 16 weeks n = 6–10, *p < 0.05. Unpaired two-tailed Student's *t* test.

(H) Immunohistochemical staining of VNUT and P2Y$_2$R in liver sections of representative mice fed with normal chow or high-fat diet for 16 weeks. Scale bar: 200 μm.

Limitations of the study

It is worth mentioning that the current study focused on hyperglycemia models, which needs to be further confirmed in standard type 1 and type 2 diabetes models. In addition, the exact molecular target underlying metformin suppression of GSAS remains to be determined. Nonetheless, we have traced it down to a disruption of the vesicular ATP release mechanism. It should be noted that metformin is a weak base, and it easily accumulates in endolysosomes and decreases their acidity, which disrupts their functions possibly including vesicular ATP uptake. Another straightforward and translational question is whether a selective P2Y$_2$R antagonist would mimic the antihyperglycemic effect of metformin. Indeed, it was reported that kaempferol, one of the antagonists for the P2Y$_2$R with an IC50 value in the low micromolar concentration,[37] has an anti-diabetes effect on a mouse model by suppressing hepatic glucose production.[38] These findings are consistent with other

reports showing that $P2Y_2R$ deficiency protects mice from hepatic steatosis[39] and glomerulonephritis.[40] Finally, it also remains to be determined whether ATP is the only nucleotide that is released in response to high glucose stimulation, though we have excluded the involvement of ADP (Figures S16–S18). However, whether other nucleotides such as UTP are released will be the object of future investigations.

STAR★METHODS

Detailed methods are provided in the online version of this paper and include the following:

- KEY RESOURCES TABLE
- RESOURCE AVAILABILITY
  - Lead contact
  - Materials availability
  - Data and code availability
- EXPERIMENTAL MODEL AND STUDY PARTICIPANT DETAILS
- METHOD DETAILS
  - Cell cultures
  - Intracellular Ca^{2+} mobilization assay
  - ATP secretion assays
  - Extracellular ADP assays
  - Intracellular ATP quantification
  - Measurement of the blood level of ATP
  - RT-PCR and Real-time PCR analysis
  - Western blotting assays
  - PIP_2 supplementation
  - In-Cell PIP_3 ELISA
  - Silencing of $P2Y_2R$ by siRNA
  - Generating HepG2 stable cell line expressing the membrane displayed ATP sensor (pm-iATPSnFR1.1)
  - Observing ATP secretion in HepG2-AS cells
  - Imaging lysosome acidification in HepG2 cells
  - Intracellular MANT-ATP accumulation
  - VNUT immunofluorescence assay
  - Gluconeogenesis assay
  - Glycogen measurement
  - Glucose uptake assay
  - Extracellular glucose quantification
  - Glucose tolerance test
  - Insulin tolerance test
  - Immunohistochemistry
- QUANTIFICATION AND STATISTICAL ANALYSIS

SUPPLEMENTAL INFORMATION

Supplemental information can be found online at https://doi.org/10.1016/j.isci.2023.106898.

ACKNOWLEDGMENTS

We thank Dr. Peter Panizzi's lab at Auburn University for assistance with cryostat liver tissue sectioning. This study was partly supported by the National Institutes of Health (1R01HL125279-01A1 to J. Shen).

AUTHOR CONTRIBUTIONS

J. Shen conceived and supervised the project. J. Senfeld performed most of the cell culture experiments, and QP performed all the *in vivo* mouse experiments. YS and SQ performed PIP_3 ELISA and immunohistochemistry studies. J. Senfeld wrote the original draft, and QP and J. Shen edited the manuscript. All authors revised and approved the final manuscript.

DECLARATION OF INTERESTS

The authors declare no competing interests.

INCLUSION AND DIVERSITY

We support inclusive, diverse, and equitable conduct of research.

Received: December 1, 2022
Revised: March 1, 2023
Accepted: May 12, 2023
Published: May 19, 2023

REFERENCES

1. The IDF Diabetes Atlas Tenth edition (2021). Diabetes Facts & Figures. https://www.idf.org/aboutdiabetes/what-is-diabetes/facts-figures.html.

2. Werner, E.A., and Bell, J.; CCXIV (1922). The preparation of methylguanidine, and of ββ-dimethylguanidine by the interaction of dicyanodiamide, and methylammonium and dimethylammonium chlorides respectively. J. Chem. Soc. Trans. *121*, 1790–1794. https://doi.org/10.1039/CT9222101790.

3. Wiernsperger, N.F., and Bailey, C.J. (1999). The antihyperglycaemic effect of metformin: therapeutic and cellular mechanisms. Drugs *58*, 31–39. https://doi.org/10.2165/00003495-199958001-00009.

4. Wheaton, W.W., Weinberg, S.E., Hamanaka, R.B., Soberanes, S., Sullivan, L.B., Anso, E., Glasauer, A., Dufour, E., Mutlu, G.M., Budigner, G.S., and Chandel, N.S. (2014). Metformin inhibits mitochondrial complex I of cancer cells to reduce tumorigenesis. Elife *3*, e02242. https://doi.org/10.7554/eLife.02242.

5. El-Mir, M.-Y., Ronique Nogueira, V., Fontaine, E., Avé Ret §, N., Rigoulet, M., and Leverve, X. (2000). Dimethylbiguanide inhibits cell respiration via an indirect effect targeted on the respiratory chain complex I*. J. Biol. Chem. *275*, 223–228. https://doi.org/10.1074/jbc.275.1.223.

6. Foretz, M., Hébrard, S., Leclerc, J., Zarrinpashneh, E., Soty, M., Mithieux, G., Sakamoto, K., Andreelli, F., and Viollet, B. (2010). Metformin inhibits hepatic gluconeogenesis in mice independently of the LKB1/AMPK pathway via a decrease in hepatic energy state. JCI *120*, 2355–2369. https://doi.org/10.1172/JCI40671.

7. Leonard, C.E., Han, X., Brensinger, C.M., Bilker, W.B., Cardillo, S., Flory, J.H., and Hennessy, S. (2018). Comparative risk of serious hypoglycemia with oral antidiabetic monotherapy: a retrospective cohort study. Pharmacoepidemiol. Drug Saf. *27*, 9–18. https://doi.org/10.1002/pds.4337.

8. Geisler, J.C., Corbin, K.L., Li, Q., Feranchak, A.P., Nunemaker, C.S., and Li, C. (2013). Vesicular nucleotide transporter-mediated ATP release regulates insulin secretion. Endocrinology *154*, 675–684. https://doi.org/10.1210/en.2012-1818.

9. Tatsushima, K., Hasuzawa, N., Wang, L., Hiasa, M., Sakamoto, S., Ashida, K., Sudo, N., Moriyama, Y., and Nomura, M. (2021). Vesicular ATP release from hepatocytes plays a role in the progression of nonalcoholic steatohepatitis. Biochim. Biophys. Acta Mol. Basis Dis. *1867*, 166013. https://doi.org/10.1016/j.bbadis.2020.166013.

10. He, L., and Wondisford, F.E. (2015). Metformin action: concentrations matter. Cell Metabol. *21*, 159–162. https://doi.org/10.1016/j.cmet.2015.01.003.

11. Tissue Expression of SLC17A9 - Summary - *the Human Protein Atlas*. https://www.proteinatlas.org/ENSG00000101194-SLC17A9/tissue.

12. Sakamoto, S., Miyaji, T., Hiasa, M., Ichikawa, R., Uematsu, A., Iwatsuki, K., Shibata, A., Uneyama, H., Takayanagi, R., Yamamoto, A., et al. (2014). Impairment of vesicular ATP release affects glucose metabolism and increases insulin sensitivity. Sci. Rep. *4*, 6689. https://doi.org/10.1038/srep06689.

13. Hasuzawa, N., Tatsushima, K., Tokubuchi, R., Kabashima, M., and Nomura, M. (2021). VNUT を標的とした 2 型糖尿病・NASH に対する創薬研究 VNUT is a therapeutic target for type 2 diabetes and NASH. Yakugaku Zasshi *141*, 517–526. https://doi.org/10.1248/yakushi.20-00204-4.

14. Ma, T., Tian, X., Zhang, B., Li, M., Wang, Y., Yang, C., Wu, J., Wei, X., Qu, Q., Yu, Y., et al. (2022). Low-dose metformin targets the lysosomal AMPK pathway through PEN2. Nature *603*, 159–165. https://doi.org/10.1038/s41586-022-04431-8.

15. Papandreou, C., Li, J., Liang, L., Bulló, M., Zheng, Y., Ruiz-Canela, M., Yu, E., Guasch-Ferré, M., Razquin, C., Clish, C., et al. (2019). Metabolites related to purine catabolism and risk of type 2 diabetes incidence; modifying effects of the TCF7L2-rs7903146 polymorphism. Sci. Rep. *9*, 2892. https://doi.org/10.1038/s41598-019-39441-6.

16. Lin, K.C., Yeh, L.R., Chen, L.J., Wen, Y.J., Cheng, K.C., and Cheng, J.T. (2012). Plasma glucose-lowering action of allantoin is induced by activation of imidazoline I-2 receptors in streptozotocin-induced diabetic rats. Horm. Metab. Res. *44*, 41–46. https://doi.org/10.1055/s-0031-1295439.

17. Jain, S., Pydi, S.P., Toti, K.S., Robaye, B., Idzko, M., Gavrilova, O., Wess, J., and Jacobson, K.A. (2020). Lack of adipocyte purinergic $P2Y_6$ receptor greatly improves whole body glucose homeostasis. Proc. Natl. Acad. Sci. USA *117*, 30763–30774. https://doi.org/10.1073/pnas.2006578117.

18. Jain, S., Pydi, S.P., Jung, Y.H., Scortichini, M., Kesner, E.L., Karcz, T.P., Cook, D.N., Gavrilova, O., Wess, J., and Jacobson, K.A. (2021). Adipocyte P2Y14 receptors play a key role in regulating whole-body glucose and lipid homeostasis. JCI Insight *6*, e146577. https://doi.org/10.1172/jci.insight.146577.

19. Solinas, G., and Becattini, B. (2017). JNK at the crossroad of obesity, insulin resistance, and cell stress response. Mol. Metabol. *6*, 174–184. https://doi.org/10.1016/j.molmet.2016.12.001.

20. Debnath, M., Agrawal, S., Agrawal, A., and Dubey, G.P. (2016). Metaflammatory responses during obesity: pathomechanism and treatment. Obes. Res. Clin. Pract. *10*, 103–113. https://doi.org/10.1016/j.orcp.2015.10.012.

21. Liu, Z., and Cao, W. (2009). p38 mitogen-activated protein kinase: a critical node linking insulin resistance and cardiovascular diseases in type 2 diabetes mellitus. Endocr. Metab. Immune Disord.: Drug Targets *9*, 38–46. https://doi.org/10.2174/187153009787582397.

22. Buxton, D.B., Robertson, S.M., and Olsont, M.S. (1986). Stimulation of glycogenolysis by adenine nucleotides in the perfused rat liver. Biochem. J. *237*, 773–780. https://doi.org/10.1042/bj2370773.

23. Hashimoto, N., Robinson, F.W., Shibata, Y., Flanagan, J.E., and Kono, T. (1987). Diversity in the effects of extracellular ATP and adenosine on the cellular processing and physiologic actions of insulin in rat adipocytes. J. Biol. Chem. *262*, 15026–15032. https://doi.org/10.1016/S0021-9258(18)48132-X.

24. PROBST, I., QUENTMEIER, A., SCHWEICKHARDT, C., and UNTHAN-FECHNER, K. (1989). Stimulation of insulin of glycolysis in cultured hepatocytes is attenuated by extracellular ATP and puromycin through purine-dependent inhibition of phosphofructokinase 2 activation. Eur. J. Biochem. *182*, 387–393. https://doi.org/10.1111/j.1432-1033.1989.tb14843.x.

25. Koike, M., Kashiwagura, T., and Takeguchi, N. (1992). Gluconeogenesis stimulated by extracellular ATP is triggered by the initial increase in the intracellular Ca2+ concentration of the periphery of hepatocytes. Biochem. J. *283*, 265–272. https://doi.org/10.1042/bj2830265.

26. Zhang, Y., Wang, Z., Zhao, Y., Zhao, M., Wang, S., Hua, Z., and Zhang, J. (2012). The plasma 5′-AMP acts as a potential upstream regulator of hyperglycemia in type 2 diabetic mice. Am. J. Physiol. Endocrinol. Metab. *302*,

325–333. https://doi.org/10.1152/ajpendo.00424.2011.

27. Keppens, S., and de Wulf, H. (1986). Characterization of the liver P2-purinoceptor involved in the activation of glycogen phosphorylase. Biochem. J. *240*, 367–371. https://doi.org/10.1042/bj2400367.

28. Keppens, S., Vandekerckhove, A., and de Wulf, H. (1992). Extracellular ATP and UTP exert similar effects on rat isolated hepatocytes. Br. J. Pharmacol. *105*, 475–479. https://doi.org/10.1111/j.1476-5381.1992.tb14278.x.

29. Keppens, S., and de Wulf, H. (1985). P2-purinergic control of liver glycogenolysis. Biochem. J. *231*, 797–799. https://doi.org/10.1042/bj2310797.

30. Cohen, S.E., Tseng, Y.H., Michael, M.D., and Kahn, C.R. (2004). Effects of insulin-sensitising agents in mice with hepatic insulin resistance. Diabetologia *47*, 407–411. https://doi.org/10.1007/s00125-003-1320-4.

31. Thorens, B. (2015). GLUT2, glucose sensing and glucose homeostasis. Diabetologia *58*, 221–232. https://doi.org/10.1007/s00125-014-3451-1.

32. Yang, X., Zhao, Y., Sun, Q., Yang, Y., Gao, Y., Ge, W., Liu, J., Xu, X., Weng, D., Wang, S., and Zhang, J. (2019). Adenine nucleotide-mediated regulation of hepatic PTP1B activity in mouse models of type 2 diabetes. Diabetologia *62*, 2106–2117. https://doi.org/10.1007/s00125-019-04971-1.

33. Enjyoji, K., Kotani, K., Thukral, C., Blumel, B., Sun, X., Wu, Y., Imai, M., Friedman, D., Csizmadia, E., Bleibel, W., et al. (2008). Deletion of Cd39/Entpd1 results in hepatic insulin resistance. Diabetes *57*, 2311–2320. https://doi.org/10.2337/db07-1265.

34. Capiotti, K.M., Siebel, A.M., Kist, L.W., Bogo, M.R., Bonan, C.D., and Da Silva, R.S. (2016). Hyperglycemia alters E-NTPDases, ecto-5′-nucleotidase, and cytosolic adenosine deaminase activities and expression from encephala of adult zebrafish (Danio rerio). Purinergic Signal. *12*, 211–220. https://doi.org/10.1007/s11302-015-9494-z.

35. Sparks, D.L., Doelle, H., and Chatterjee, C. (2014). Circulating nucleotides in Health and disease. Recept. Clin. Investig. *1*, e344. https://doi.org/10.14800/RCI.344.

36. Wilcock, C., and Bailey, C.J. (1994). Accumulation of metformin by tissues of the normal and diabetic mouse. Xenobiotica *24*, 49–57. https://doi.org/10.3109/00498259409043220.

37. Kaulich, M., Streicher, F., Mayer, R., Müller, I., and Müller, C.E. (2003). Flavonoids — novel lead compounds for the development of $P2Y_2$ receptor antagonists. Drug Dev. Res. *59*, 72–81. https://doi.org/10.1002/ddr.10203.

38. Alkhalidy, H., Moore, W., Wang, Y., Luo, J., McMillan, R.P., Zhen, W., Zhou, K., and Liu, D. (2018). The flavonoid kaempferol ameliorates streptozotocin-induced diabetes by suppressing hepatic glucose production. Molecules *23*, 2338. https://doi.org/10.3390/molecules23092338.

39. Dusabimana, T., Park, E.J., Je, J., Jeong, K., Yun, S.P., Kim, H.J., Kim, H., and Park, S.W. (2021). P2y2r deficiency ameliorates hepatic steatosis by reducing lipogenesis and enhancing fatty acid β-oxidation through ampk and pgc-1α induction in high-fat diet-fed mice. Int. J. Mol. Sci. *22*, 5528. https://doi.org/10.3390/ijms22115528.

40. Rennert, L., Zschiedrich, S., Sandner, L., Hartleben, B., Cicko, S., Ayata, C.K., Meyer, C., Zech, A., Zeiser, R., Huber, T.B., et al. (2018). P2Y2R signaling is involved in the onset of glomerulonephritis. Front. Immunol. *9*, 1589. https://doi.org/10.3389/fimmu.2018.01589.

41. Lobas, M.A., Tao, R., Nagai, J., Kronschläger, M.T., Borden, P.M., Marvin, J.S., Looger, L.L., and Khakh, B.S. (2019). A genetically encoded single-wavelength sensor for imaging cytosolic and cell surface ATP. Nat. Commun. *10*, 711. https://doi.org/10.1038/s41467-019-08441-5.

42. Ding, L., Ma, W., Littmann, T., Camp, R., and Shen, J. (2011). The P2Y2 nucleotide receptor mediates tissue factor expression in human coronary artery endothelial cells. J. Biol. Chem. *286*, 27027–27038. https://doi.org/10.1074/jbc.M111.235176.

43. Ma, W., Liu, Y., Ellison, N., and Shen, J. (2013). Induction of C-X-C chemokine receptor type 7 (CXCR7) switches stromal cell-derived factor-1 (SDF-1) signaling and phagocytic activity in macrophages linked to atherosclerosis. J. Biol. Chem. *288*, 15481–15494. https://doi.org/10.1074/jbc.M112.445510.

44. Ma, W., Liu, Y., Wang, C., Zhang, L., Crocker, L., and Shen, J. (2014). Atorvastatin inhibits CXCR7 induction to reduce macrophage migration. Biochem. Pharmacol. *89*, 99–108. https://doi.org/10.1016/j.bcp.2014.02.014.

45. Liu, Y., Zhang, L., Wang, C., Roy, S., and Shen, J. (2016). Purinergic P2Y2 receptor control of tissue factor transcription in human coronary artery endothelial cells: new AP-1 transcription factor site and negative regulator. J. Biol. Chem. *291*, 1553–1563. https://doi.org/10.1074/jbc.M115.681163.

STAR★METHODS

KEY RESOURCES TABLE

REAGENT or RESOURCE	SOURCE	IDENTIFIER
Antibodies		
Anti-AKT	Cell Signaling	#9272
Anti-p-AKT (S473)	Cell Signaling	#9271
Anti-p-AKT (T308)	Cell Signaling	#13038
Anti-ERK1/2	Cell Signaling	#4695
Anti-p-ERK1/2	Cell Signaling	#4370
Anti-p38	Cell Signaling	#8690
Anti-p-p38	Cell Signaling	#4511
Anti-JNK	Cell Signaling	#9252
Anti-p-JNK	Cell Signaling	#4668
Anti-p-AMPKα (T172)	Cell Signaling	#50081
Anti-AMPKα	Cell Signaling	#5832
Anti- GSK3β	Cell Signaling	#9315
Anti-p-GSK3β (S9)	Cell Signaling	#9323
Anti-GAPDH	Cell Signaling	#2118
Biotinylated anti-PIP3 IgM	Echelon	#Z-B345
Anti-P2Y2R	Abclonal	#A13923
Anti-VNUT	Proteintech	#26731-1-AP
Rabbit anti-mouse IgG (light chain specific) secondary antibody, HRP	Cell Signaling	#58802
Goat anti-rabbit IgG (H+L) secondary antibody, HRP	ThermoFisher Scientific	#31460
Bacterial and virus strains		
iATPSnFR1.1	Lobas et al.[41]	Addgene #102549
Chemicals, peptides, and recombinant proteins		
EMEM	Lonza	12-611Q
Opt. MEM	Gibco	11058021
Depleted DMEM	Lonza	A1443001
Fetal bovine serum	ThermoFisher Scientific	A5256701
DMSO	EMD Milipore	102952
ATP disodium salt	MilliporeSigma	A1852
UTP disodium salt	MilliporeSigma	94370
UDP disodium salt	Tocris	3111
ATPγS	Jena Bioscience	NU-406
UTPγS	Jena Bioscience	NU-416
ADPβS	Jena Bioscience	NU-433
NF546	Tocris	3892/10
ARC-118925XX	Tocris	4890/5
ARL67156 trisodium salt	Tocris	1283/10
A23187, free acid	Tocris	1234/10
Metformin	Enzo Life Sciences	50-200-8556
Phenformin HCl	BioVision	1889

(*Continued on next page*)

Continued

REAGENT or RESOURCE	SOURCE	IDENTIFIER
Buformin HCl	Cayman Chemical	18507
Proguanil HCl	MilliporeSigma	G7048
Bafilomycin A1	Enzo	BML-CM110-0100
Allantoin	Cayman Chemical	30204
PBS (10x)	VWR	J373-4L
SYBR Green PCR master mix	Applied Biosystems	4309155
4X Laemmli Sample Buffer	Bio-Rad	1610747
TG-SDS (10x)	VWR	0783-5L
TBS (10x)	ThermoFisher Scientific	J60764-k7
TAE (10x)	VWR	J63677
Tween 20	VWR	M147-1L
DharmaFECT-1	Dharmacon / Horizon Discovery	T-2001-03
G418	EMD Milipore	345812
Hematoxylin	VWR	517-28-2
Eosin	VWR	10863-274
Bluing Reagent	Richard-Allan Scientific	7301
U73122	Tocris	1268
Monensin sodium salt	Enzo Life Sciences	ALX-380-026-G001
D-Glucose	VWR	AAJ60067-AK
Mannitol	VWR	A14030
LysoView 633	Biotium	70058-T
MemGlow640	MemBright	MG04
MemGlow488	MemBright	MG01
Mini-protean TGX gels	Bio-Rad	4561033
MANT-ATP	ThermoFisher Scientific	M12417
Insulin (Humulin® U-100)	Eli Lilly	NDC 54868-3619-0
HEPES	MilliporeSigma	H4034
Critical commercial assays		
Fluorforte Calcium Mobilization Assay	Enzo Life Science	ENZ-51016
ENLIGHTEN ATP Assay	Promega	FF2000
Colorimetric/fluorometric ATP Assay	Abcam	ab83355
Amplex Red Glucose Assay	Invitrogen	A12222
Glycogen Detection Assay	Cayman Chemical	700480
Glucose Uptake Assay	Abcam	ab136956
ADP Assay Kit	Sigma-Aldrich	MAK133
RNeasy Mini Kit	Qiagen	74104
Experimental models: Cell lines		
HepG2 cells	ATCC	HB-8065
Primary Human Hepatocytes	Applied Biological Materials Inc.	T0051
Experimental models: Organisms/strains		
B6.129P2-P2ry2 tm1Bhk /J (mice)	Jackson Laboratory	009132
C57BL/6NJ (mice)	Jackson Laboratory	005304
Oligonucleotides		
ON-TARGET plus SMART Pool L-003688-00-0005 (human P2RY2, NM_002564)	Dharmacon	L-003688-00-0050

(*Continued on next page*)

Continued

REAGENT or RESOURCE	SOURCE	IDENTIFIER
ON-TARGET plus Non-targeting Control Pool	Dharmacon	D-001810-10-20
Software and algorithms		
Prism 9	GraphPad	https://www.graphpad.com/
ImageJ	NIH	https://imagej.net/ij/index.html
Excel	Microsoft Office	https://www.microsoft.com/en-us/microsoft-365
BioRender	Online	https://biorender.com/
Other		
True Metrix Go® glucometer	Trividia Health	KRKY0184203431
VectaMount® AQ Aqueous Mounting Medium	Vector® Laboratories	H-1800
Standard chow diet	ENVIGO	TD.08485
High-fat diet	ENVIGO	TD.88137
AMG EVOS digital inverted microscopy	ThermoFisher Scientific	AMEX1000

RESOURCE AVAILABILITY

Lead contact

Further information and requests for resources and reagents should be directed to and will be fulfilled by the lead contact, Jianzhong Shen (jzs0019@auburn.edu).[41]

Materials availability

This study did not generate any new reagents.

Data and code availability

- All data reported in this paper will be shared by the lead contact upon request.
- This paper does not report the original code.
- Any additional information required to re-analyze the data reported in this paper is available from the lead contact upon request.

EXPERIMENTAL MODEL AND STUDY PARTICIPANT DETAILS

Mice homozygous for inactivation of the $P2Y_2R$ gene ($P2Y_2R$ KO, Jackson Laboratory) were back-crossed more than 10 generations into the C57BL/6 background. At 4 weeks, age-matched male mice ($P2Y_2R$-KO versus $P2Y_2R$-WT) were fed either a standard chow diet (ENVIGO) or a high-fat diet (Fat: 42% of total Kcal; Sucrose: 34.5% of total weight; Saturated fatty acid: 66% of all fat; ENVIGO) for another 16 weeks before being used for experiments. All mice were maintained in a facility free of well-defined pathogens under the supervision of the Biological Resource Unit at Auburn University. All animal protocols were approved by Auburn Institutional Animal Care and Use Committee, and the investigation conforms to the Guide for the Care and Use of Laboratory Animals published by the United States National Institutes of Health.

METHOD DETAILS

Cell cultures

HepG2 cells were filtered by 70 μm cell strainers and grown in a monolayer, cultured in EMEM (also called MEM) supplemented with 10% FBS at 37°C in a humidified atmosphere of 5% CO_2. Primary human hepatocytes (PHH) were also cultured in EMEM supplemented with 10% FBS at 37°C in a humidified atmosphere of 5% CO_2. Before stimulation, cells were seeded to grow for 24 h, reaching ~80–90% confluence, and starved for 3 h, 6 h, or overnight. When inhibitors or antagonists were used, cells were pretreated with the inhibitor/antagonist for 35min to 1 h before cell stimulation by different agonists at the specified times and concentrations.

Intracellular Ca^{2+} mobilization assay

Cells were seeded at a density of $4x10^4$ per well into 96-well culture plates and cultured for one day. On day two, the original medium was removed. The assay medium from the FluoForte™ kit containing the Ca^{2+} dye was added, and receptor-mediated Ca^{2+} mobilization was determined as we previously described.[42] Fluorescence was determined immediately after adding different reagents, with an excitation wavelength set to 490 nm and an emission wavelength set to 525 nm, and readings were taken every 1s for 640s. For the antagonist inhibition experiment, cells were pre-incubated with the antagonist for 45 min before agonist addition. Measurement of Ca^{2+} signal was performed with the fluorometer plate reader (B.M.G. FLUOstar), the results of which were shown as relative fluorescence units (RFU).

ATP secretion assays

Luminescent method

ATP secretion from hepatocytes was quantified utilizing ENLIGHTEN ATP Assay System Bioluminescence Detection Kit (Promega). Hepatocytes were cultured in a 6-well plate 24 h before experimentation and starved for 3-5 h before the start of the experiment. NTPDase inhibitor ARL67156 (Tocris) was added to every well at a concentration of 100μM for 30 min to inhibit the enzymes that degrade extracellular ATP. Compounds metformin, phenformin, buformin, proguanil, monensin, bafilomycin, clodronate, and allantoin were pretreated for 35 min at concentrations from 10 nM to 30 μM before supplementing 5- or 25 mM D-glucose. Measurement of extracellular ATP was accomplished by combining 100 μL assay reagent with 100 μL medium extracted from each well in a white 96-well plate. Quantification was completed in a Glomax 96 microplate luminometer (Promega), resulting in data being presented as relative light units (RLU).

Fluorometric method

ATP secretion from hepatocytes was also quantified utilizing a colorimetric/fluorometric ATP Assay Kit (Abcam). Hepatocytes were cultured in a 6-well plate for 24 h and then starved for 3-6 h before the start of the experiment. Additionally, NTPDase inhibitor ARL67156 was first added to every well at a concentration of 100 μM for 30 min. Compound metformin was pretreated for 35 min at concentrations from 1 μM to 30 μM before supplementing 5- or 25 mM D-glucose. Extracellular ATP was measured by combining 50 μL assay reagent with 50 μL medium extracted from each well in a black/transparent bottom 96-well plate (Greiner), incubated in darkness at room temperature for 30 min. Data was collected from a 96-well plate reader using Ex/Em = 535/587nm and reported in relative fluorescent units (RFU).

Extracellular ADP assays

Extracellular ADP levels were evaluated similarly to the "ATP secretion assay". Briefly, 1 mL cell culture medium was taken after a high glucose challenge of the cultured HepG2 cells for 30 min or 60 min with or without ARL67156 pretreatment for 30 min. ADP levels were then quantified with the "ADP assay kit" (Sigma-Aldrich) following the manufacturer's protocol. 90 μL of a reaction mix containing reaction buffer, luciferin, and firefly luciferase were mixed with 10 μL of the samples and the luminescence was quantified in a luminometer to determine the RLU_{ATP}. Subsequently, the "ADP enzyme" was added to the samples, and the luminescence was measured again after a 2-min incubation to determine the RLU_{ADP}. The luminescence corresponding to ADP was calculated (RLU_{ADP}-RLU_{ATP}), with the final data presented as RLU.

Intracellular ATP quantification

Hepatocytes were plated in 6-well plates containing the growth medium at 80% confluency. ATP quantity in hepatocytes was determined utilizing a colorimetric/fluorometric ATP Assay Kit (Abcam). Before performing the ATP quantification assay, a fresh serum-free culture medium was added to every well for 3-6 h and then treated with 30 μM metformin or PBS for 2 h. Cell lysates were then collected using the Deproteinizing Sample Preparation Kit (Abcam). ATP quantity in the cell lysates was determined based on the phosphorylation of glycerol to generate a product detectable by fluorometry or absorbance. Briefly, 50 μL assay reagent was mixed with 50 μL lysate in a transparent bottom 96-well plate and incubated in darkness at room temperature for 30 min. ATP concentration was then determined by measuring absorbance at OD 570 nm (colorimetric). The results are shown as absorbance (abs).

Measurement of the blood level of ATP

Mice were pretreated for 15 min with saline (0.9% NaCl) or metformin (50mg/kg, i.v.) through tail vein injection, after which 5 uL of tail blood was mixed with 45 uL saline to minimize platelet activation. The baseline level of ATP in the diluted blood sample was immediately measured by the luciferin-luciferase assay as previously described. Then, mice were injected intraperitoneally with D-glucose (1.5g/kg body weight) in normal saline (0.9% NaCl) or just saline as a control. Blood samples were further collected after 30 min and 60 min of D-glucose injection, and measurement of ATP was executed by combining 50 μL assay reagent with 50 μL diluted blood in a white 96-well plate. Quantification was accomplished in a Glomax 96 microplate luminometer (Promega), resulting in data being presented as relative light units (RLU).

RT-PCR and Real-time PCR analysis

RT-PCR and Real-time PCR were carried out as we previously reported.[43] Briefly, total RNA and DNA were extracted from HepG2 or PHH cells using the RNeasy and DNeasy kits, respectively. On-column DNA digestion was carried out during RNA extraction. For the synthesis of the first strand of cDNA, 1 μg of total RNA after DNase treatment was reverse transcribed using a cDNA synthesis kit. Real-time PCR was performed on a CFX96 detection system (Bio-Rad) with SYBR Green reagents (Qiagen). All PCR primers' sequences are listed below: $P2Y_1$, forward: 5′- TGG CGG GAG ATA CTT TCA -3′, reverse: 5′-GGA GAT TCT TGT GCC TTC AC -3′; $P2Y_2$, forward: 5′- CCT CAA GAC CTG GAA TGC GT -3′, reverse: 5′- TGG AAT GGC AGG AAG CAG AG-3′; $P2Y_4$, forward: 5′- TCT ATA AAG TGA CTC GGC CC -3′, reverse: 5′-GGC TTC CCG TGT TAC AAT-3′; $P2Y_6$, forward: 5′- TGG GCA GCC ATG GAA T-3′, reverse: 5′- CTG GGG CTC TGA CGG TTT AG-3′; $P2Y_{11}$, forward: 5′- GCG GCC TAC AGA CGC TAT AG-3′, reverse: 5′-CTG GGG CTC TGA CGG TTT AG-3′; $P2Y_{12}$, forward: 5′-ATG CAA GCC GTC GAC AAC CT -3′, reverse: 5′-TTA CAT TGG AGT CTC TTC ATT TG-3′; $P2Y_{13}$, forward: 5′-GGT GAC ACT GGAAGC AAT -3′, reverse: 5′-ACC CAC AGA GCC AAA GTA -3′; $P2Y_{14}$, forward: 5′- CTC ATT ACA GCT GCC AGT-3′, reverse: 5′- TTG GAA GAG GGT AGG AAC TC-3′; GAPDH, forward: 5′-TCA ACA GCG ACA CCC ACT CC -3′, reverse: 5′-TGA GGT CCA CCA CCC TGT T-3′.

Western blotting assays

Western blotting was carried out as we previously reported.[44] Briefly, after the cells were stimulated for 10 min or indicated times, the cells were quickly lysed with lysis buffer. Samples were loaded into gel wells for electrophoresis, and proteins were transferred from the gel to the PVDF membrane. The individual primary antibodies used were anti-p-AKT (S473/T308), anti-p-ERK1/2, anti-p-p38, and anti-p-JNK (1:1000). Equal protein loading was verified by stripping off the original antibodies and re-probing the membranes with the primary antibody β-actin, GAPDH, total AKT, ERK1/2, p38, or JNK (1:1000). Band densitometry was quantified using ImageJ (NIH), and the ratio-metric calculations were performed in Microsoft Excel and exported to Prism9 for graphing.

PIP_2 supplementation

PIP_2 uptake optimization

HepG2 cells were supplemented with PIP_2 utilizing a PIP_2 shuttle assay kit (Echelon Biosciences). To optimize the cellular loading of PIP_2, first, PIP_2-BODIPY was mixed with a histone H1-TMR carrier at a 1:1 ratio for 15 min at room temperature, vortexing periodically. The fluorophore-bound PIP_2 complex was diluted to 25 μM in serum-free EMEM. HepG2 cells were then incubated in the complex-containing medium and imaged every 15 min using an EVOS fluorescent imaging system's GFP and RFP filter to determine the optimal time for PIP_2-BODIPY uptake.

PIP_2 treatment for western blotting

HepG2 cells were seeded in 6- or 12- well plates for at least 24 h and cultured in serum-free EMEM 4-6 h before the experiment. HepG2 cells were then treated with 25 μM non-fluorescent PIP_2-Histone H1 for 30 min, then treated with 1 nM insulin, 100μM nucleotide, or a combination for 10 min. The cells were then lysed and prepared using the aforementioned western blot protocol.

In-Cell PIP_3 ELISA

HepG2 cells were seeded in a 96-well plate and starved in a serum-free medium for 16 h before stimulation. Insulin and ATP/UTP were added to the assay wells in the indicated doses incubating for 5 min at 37°C (the PIP3 kinase inhibitor wortmannin was pre-added for 30 min as a positive control). Then, removed the

starvation medium and fixed the cells with Fixation Buffer (4% formaldehyde and 0.2% glutaraldehyde in PBS) for 15 min at room temperature. Cells were rinsed three times with cold Wash Buffer (50 mM NH4Cl in PBS) and treated with Buffer 1 Plus (Buffer 1 supplemented with 5% normal goat serum, 0.5% saponin and 50 mM NH4Cl) for 45 min on ice in order to block and permeabilize the cells. Next, removed Buffer 1 Plus and added Buffer 2 (20 mM PIPES, pH6.8, 137 mM NaCl, 2.7 mM KCl, 5% normal goat serum, 0.1% saponin) with Mouse Biotinylated Anti-PI (3,4,5)P3 IgM at 1:200 dilution. After 60 min incubation on ice, fixed cells were rinsed once with Buffer 1 (20 mM PIPES, pH6.8, 137 mM NaCl, 2.7 mM KCl) and three times with Wash Solution. Dried the plate and added prepared Streptavidin Solution, incubating for 45 min at room temperature with gentle shaking. Cells were then rinsed with Wash Solution four times and incubated with TMB One-Step Substrate Reagent (RayBiotech) for 30 min at room temperature in the dark with gentle shaking. Finally, Stop Solution was added to each well and immediately read the absorbance at 450 nm in SpectraMax® iD3 Multi-Mode Microplate Reader.

Silencing of $P2Y_2R$ by siRNA

To knock down $P2Y_2R$ expression, HepG2 cells were transfected with the four-sequence pool (ON-TARGET plus SMART pool L-003688-00-0005, human $P2Y_2R$, NM_002564, Dharmacon) using DharmaFECT-1 Transfection reagent following the manufacturer's protocol as we previously reported 38. Briefly, HepG2 cells were seeded in 6-well plates at 80–90% confluence; the medium was replaced with complete MEM without antibiotics before transfection. DharmaFECT 1 and siRNA products were incubated separately in MEM at room temperature for 5 min. Mixtures were combined, incubated for another 20 min, and added to cells at a final concentration of 2 μL/mL DharmaFECT 1 and 25 nM siRNAs. Real-time PCR assays were performed to confirm the decrease of $P2Y_2R$ mRNA after 48 h post-transfection. For ATP and UTP stimulation, siRNA and transfection reagent were removed 16 h post-transfection, and a complete culture medium was added. Experiments were performed 72 h post-transfection.

Generating HepG2 stable cell line expressing the membrane displayed ATP sensor (pm-iATPSnFR1.1)

The purchased plasmid in bacteria as agar stab for the membrane-displayed ATP sensor for mammalian cells (pm-iATPSnFR1.1) was amplified in LB cultured medium with ampicillin antibiotic at a final concentration of 100 μg/mL. Maxi Plasmid Isolation Kit (Qiagen) was used to isolate and purify the plasmids, of which the sequence was verified by sequencing, and the concentration/purity was measured through NanoDrop2000. The purified plasmids were transfected into HepG2 cells using Optimum MEM medium and Lipofectamine® 3000 Transfection Reagent, after which a stable cell line (HepG2-AS) was produced by G418 selection at 700 ng/mL for two weeks, followed by 400ng/mL for one week until hepatocytes begin growing at a standard rate, then a maintenance dose of G418 at 100ng/mL was used. A functional plasma membrane ATP sensor was verified using the EVOS fluorescent imaging system with the GFP filter, showing the green fluorescent signals at the cellular plasma membrane when the cells were challenged with 30 μM extracellular ATP or 25mM glucose.

Observing ATP secretion in HepG2-AS cells

HepG2-AS cells were cultured in EMEM containing 10% FBS and 100ng/mL G418 in a 6- or 12-well plate for 24 h at 70% confluence and then serum starved in antibiotic-free EMEM for 3-5 h before beginning the experiment. NTPDase inhibitor ARL67156 was added to all wells at a concentration of 100μM for 35 min to control for enzymatic ATP degradation across the treatment conditions. Cells were pretreated with 30 μM metformin or a PBS vehicle for 35 min before supplementing 5- or 25 mM D-glucose. HepG2-AS cells were then incubated at 37° C for 1 h and then imaged. Elevated concentrations of extracellular ATP promoted plasma membrane fluorescence of the ATP sensor, which was observed and captured using an EVOS fluorescent imaging system with the GFP filter.

Imaging lysosome acidification in HepG2 cells

Preparation of pH-sensitive LysoView™ 633 (Biotium)

Lyophilized powder was briefly centrifuged and resuspended in Milli-Q-H2O to generate a 1000X stock solution.

Performing lysosome imaging

HepG2 cells were plated in a 6- or 12-well plate after being strained through a 70 μm cell strainer and grown into a monolayer for 24 h. On the day of the experiment, cells were serum-starved for 3-6 h and then pre-treated with 30 μM metformin or a PBS vehicle for 35 min before supplementing 5- or 25 mM D-glucose. 30 min following D-glucose supplementation LysoView™ 633 at the final concentration of 1X and CellBrite® Green (Biotium) diluted 1:200 was added to each well and incubated for 30 min at 37° C then imaged using an EVOS fluorescent imaging system with the Cy5 and GFP filters.

Intracellular MANT-ATP accumulation

HepG2 cells were plated in a 6- or 12-well plate the day before the experiment and were serum-starved 3-6 h prior to pretreatment with 30 μM metformin or a PBS vehicle for 35 min. The HepG2 cells were then supplemented with 1.5 mM MANT-ATP and incubated for 25 min at 37°C before being imaged using an EVOS fluorescent imaging system with the GFP filter. The captured images were then inverted into black and white using ImageJ.

VNUT immunofluorescence assay

Cell immunofluorescence assay was carried out as we previously reported.[45] Briefly, HepG2 cells were seeded in 8-chamber glass slides (Nunc), starved for 6 hr, and then the cells were fixed for 15 min in cold methanol. The fixed cells were washed with PBS three times and blocked with 5% horse serum for 1 hr at room temperature. Then the cells were incubated with a rabbit anti-human SLC17A9 (VNUT) antibody (Proteintech) at 1:100 dilution overnight at 4°C, followed by incubation with an anti-rabbit IgG F(ab) fragment conjugated with AF-488 (Cell Signaling) at 1:1000 dilution for 90 min at room temperature in darkness. For negative controls, cells were incubated with non-immune rabbit IgG in place of the primary antibody or only the AF-488-conjugated secondary antibody. Cells were washed with PBS three times before a mounting medium containing DAPI was added to seal the slides. Images with fluorescent signals in random fields were acquired and captured using an AMG EVOS digital inverted multifunctional microscope.

Gluconeogenesis assay

Cell-released glucose via gluconeogenesis was quantified using the Amplex Red Glucose Assay Kit (Invitrogen™) as detailed below:

Cell culture and medium sample preparation

HepG2 cells were seeded in a 6-well plate, and treatment wells were duplicated to monitor gluconeogenesis and another to control for background glucose production. Hepatocytes grew in a monolayer, reaching approximately 85% confluency. After reaching confluency, starve hepatocytes in serum-free EMEM for 6 h. The base medium utilized was DMEM free of serum, phenol red, glucose, pyruvate, glutamate, and lactate. Both glucose production and background medium required HEPES to be added to the medium at a concentration of 10 mM. The glucose production medium was made by supplementing sodium lactate at a concentration of 10mM. The background medium possessed no gluconeogenic substrates. The $P2Y_2R$ antagonist ARC-118929XX and ectonucleotidase inhibitor ARL-67156 were added 45 min before removing the starvation medium. While hepatocytes were starving, a cocktail containing treatment and inhibitors was prepared, after which we removed the starvation medium, washed the cells with PBS pre-warmed to 37°C, and then added 350 μL pre-made cocktail medium to the appropriate wells to incubate for 3.5 h before collecting medium for glucose quantification.

Reagent preparation for Amplex Red glucose assay

Before using, dissolve the Amplex Red vial in 60 μL DMSO – the final reaction volume is 100 μL. Prepare 1X reaction buffer by adding 4 mL of 5X reaction buffer to 16 ml dH2O producing a total volume of 20 mL (~100 assays). Next, a 10U/mL stock solution of horseradish peroxidase (HRP) is prepared (1U is the amount of enzyme that will form 1.0 mg purpurgallin from pyrogallol in 20 sec, pH 6 and 20°C) by dissolving 1 mL of 1X reaction buffer. Prepare a 100U/mL glucose oxidase stock solution (1U amount of oxidase 1umole of β-d-glucose to glucuronolactone and H_2O_2 per 1 min, pH 5.1, 30°C), dissolving the content of the glucose oxidase vial in 1 mL of 1X reaction buffer. Produce a 400 mM stock solution of glucose (72 mg/mL) and a stock of 20 mM H_2O_2 by diluting 3% H2O2 into the appropriate volume of 1X reaction buffer (22.7 μL of 3% H_2O_2 in 977 μL 1X reaction buffer).

Performing the Amplex Red glucose assay

Prepare a glucose standard curve (0-200 μM) in 1X reaction buffer with a total volume of 50 μL. The positive control is generated by diluting the 400 mM glucose stock to 200 μM in a 1X reaction buffer. There is also an H_2O_2 positive control created by diluting 20 mM H_2O_2 to 10 μM in 1X reaction buffer. The negative control is 1X reaction buffer without H_2O_2. *In vitro* samples require no dilution prior to reaction. Transfer 50 μL of sample supernatant into their respective wells, ensuring to do a minimum of triplicates. Next, combine 50 μL 100 μM Amplex Red, 100 μL 0.2 U/mL HRP, 100 μL 2U/mL glucose oxidase, and 4.75 mL 1X reaction buffer. Add 50 μL of the Amplex Red cocktail into all wells and allow to incubate protected from light for 30 min at room temperature. Read plate (λab: 571 nm, λem: 585 nm).

Glycogen measurement

Cellular glycogen content was evaluated using the Glycogen Assay Kit (Cayman Chemical) according to the manufacturer's instructions. Briefly, HepG2 cells were seeded in the growth medium in 6-well plates reaching about 80% confluency, and then the cells were serum-starved for 6 h. Before lysing cells, immediately dunk the plate in ice-cold PBS, knock off residual PBS, and carefully snap-freeze the 6-well plate in liquid nitrogen. Add 200 μL of premixed 1% Triton-X lysis buffer, vigorously scrape each well, and mechanically lyse cells using a 20-gauge syringe at 4°C. Then, transfer the samples into a 1.5ml Eppendorf tube, centrifuge at 15,000 rpm for 10 min at 4°C, and collect the supernatant. After that, 10 μL of cell lysates were added to every well of the 96 wells plate, and then 50 μL of hydrolysis buffer with amyloglucosidase was added to convert glycogen to β-D-glucose. Glucose oxidase was then added to convert β-D-glucose to hydrogen peroxide. Horseradish peroxidase was added, and H_2O_2, in the presence of it, reacted with 10-acetyl-3,7-dihydroxyphenoxazine to produce resorufin, whose fluorescence was measured at Ex/Em of 535/590nm. Data was analyzed based on the standard curve constructed by the kit-provided glycogen standards.

Glucose uptake assay

Samples were processed as detailed in the manual of the 2-NBDG Glucose Uptake Assay Kit (Abcam). Briefly, hepatocytes were plated in EMEM medium in 6-well plates reaching about 80% confluency, and then the cells were serum-starved for 6 h. Following starvation, replace the serum-free medium with pre-warmed glucose-free DMEM, and hepatocytes were treated with ATP or UTP for 30 min in total, during which the final 10 min of the cells were incubated with 2-NBDG at the final concentration of 200 μg/mL. After NBDG was taken up by the cells, fluorescence was determined immediately with an excitation wavelength set to 485 nm and an emission wavelength set to 535 nm.

Extracellular glucose quantification

The extracellular level of glucose was determined using the Glucose Assay Kit (Abcam). Briefly, HepG2 cells were seeded in a 6-well plate, reaching approximately 85% confluency, after which the cells were starved in serum-free EMEM for 6 h. A standard curve for glucose was produced using the range 0-300 mg/dL. 5 μL of sample supernatants and standards were transferred to 1.5 mL tubes. Add 500 μL of acetic acid-based reagent, close the lids very tightly, and vortex. Notably, due to the acetic acid present in the reagents, this experiment was predominately performed in fume hood—transfer tubes to either a heat block at 100°C or a boiling water bath for 8 min. Immediately transfer the tubes to a cool water bath or ice for 4 min. After cooling, transfer 200 μL of the sample, standard, and pure water (blank) to a 96-well plate—measure optical density (OD) at 630 nm. Data were analyzed based on the standard curve constructed by the kit-provided glucose standards.

Glucose tolerance test

Mice were fasted for 12 h with free access to drinking water. Each mouse then received an intraperitoneal injection of filter-sterilized D-glucose (1.5g/kg body weight) in normal saline (0.9% NaCl). Blood glucose levels were measured using a glucose meter (True Metrix Go® glucometer, TRIVIDIA HEALTH) from tail blood at 0, 15, 30, 60, 90, and 120 min after intraperitoneal injection of glucose solution.

Insulin tolerance test

After 6 h fasting with free access to drinking water, mice were given intraperitoneal injections of human insulin (Humulin® U-100, Eli Lilly) at a dose of 0.75 IU/kg body weight using a sterile insulin syringe. Blood

glucose levels were determined using a glucose meter (True Metrix Go® glucometer, TRIVIDIA HEALTH) from tail blood at 0, 15, 30, 60, and 90 min after insulin injection.

Immunohistochemistry

After euthanizing the mice, the liver was isolated and fixed in 10% neutral buffered formalin. The fixed liver was then refrigerated at 4°C. After 48 h refrigeration, the liver was transferred to a 30% sucrose solution in PBS, allowing the liver to soak for 48 h in the sucrose solution before sectioning. The liver tissue was then dried and integrated into a mold of frozen section compound (FSC, Surgipath). Liver sections were collected at 10 μm and attached to charged slides (Leica). Slides were then left at room temperature for 1 h before storing at -20°C. The liver tissue slides were stained using the Super Plus TM High Sensitive and Rapid Immunohistochemical Kit (Elabscience) according to the kit's instructions. Briefly, mouse liver tissue slides were placed in an Antigen Retrieval working solution for 30 min to repair the antigen. Slides were blocked with peroxidase blocking buffer at room temperature for 15 min to eliminate endogenous peroxidase activity, then washed with PBS three times for 2 min. The primary anti-$P2Y_2R$(ABclonal) or anti-VNUT antibody (Proteintech) with a 1:400 dilution using antibody dilution buffer was added to the slides and incubated at 37°C for 1 h, then washed with PBS three times for 2 min. A vehicle incubation without a primary antibody was used as a control. A drop of Poly-peroxidase-anti-Rabbit/Mouse IgG was added to the slides and incubated at 37°C for 30 min, then washed with PBS three times for 2 min. A drop of coloration solution was added to the slides, and the color tan or brownish yellow appeared. Slides were washed with deionized water at the same time to terminate the chromogenic reaction, after which the sections were counter-stained with Hematoxylin and cover-slipped with VectaMount® AQ Aqueous Mounting Medium (Vector® Laboratories). All images were then acquired and captured with SWIFTCAM Microscope Digital Camera SC1630.

QUANTIFICATION AND STATISTICAL ANALYSIS

All data were analyzed by Prism 9 (GraphPad Software Inc). Data are expressed as the mean ± SEM. The means of two groups were compared using Students t-test (unpaired, two-tailed), and one-way analysis of variance was used for the comparison of more than two groups with $p < 0.05$ considered to be statistically significant. Unless otherwise indicated, all experiments were repeated at least three times.